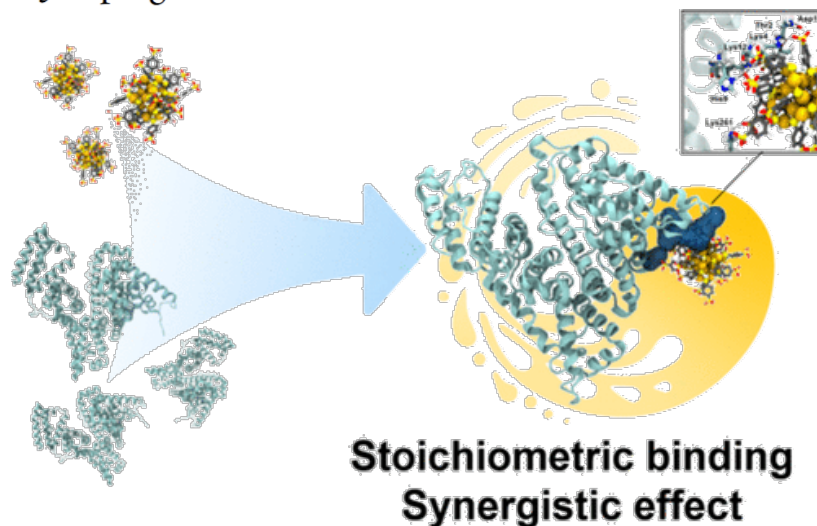


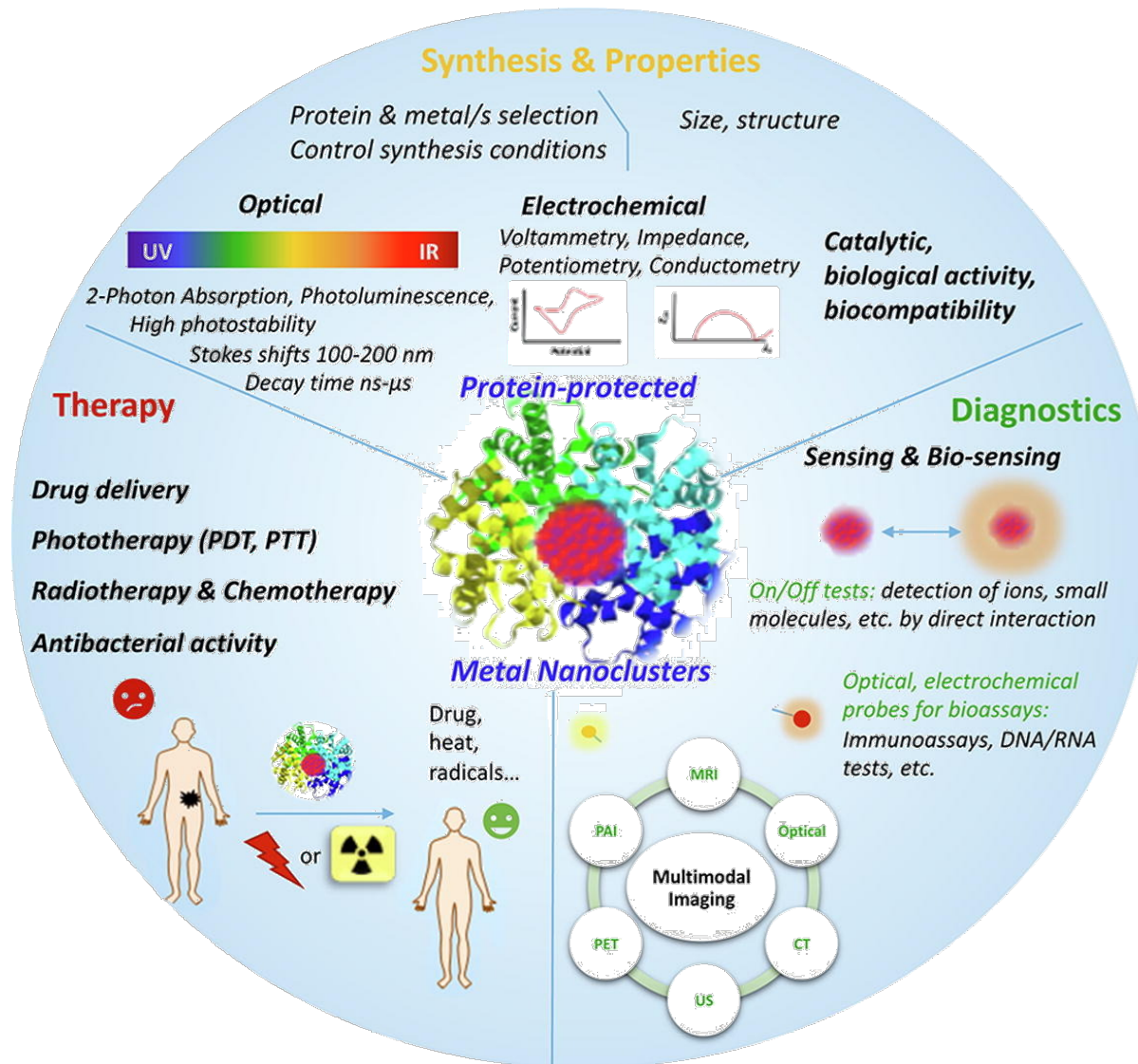
Unraveling the Stoichiometric Interactions and Synergism between Ligand-Protected Gold Nanoparticles and Proteins

Bihan Zhang,[◆] María Francisca Matus,[◆] Qiaofeng Yao,^{*} Xiaorong Song, Zhennan Wu, Wenping Hu,^{*} Hannu Häkkinen,^{*} and Jianping Xie^{*}



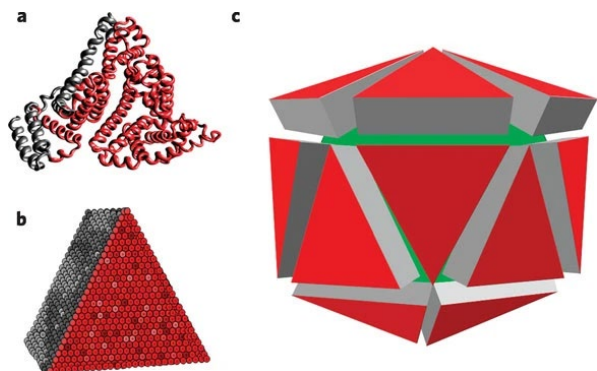
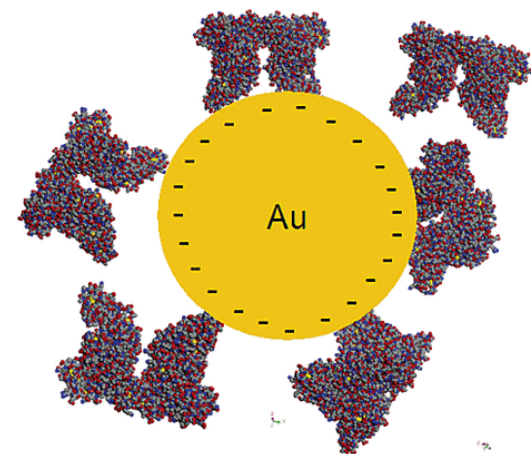
- Jianping Xie - Department of Chemical and Biomolecular Engineering, National University of Singapore, Singapore; Joint School of National University of Singapore and Tianjin University, China
- Hannu Häkkinen - Departments of Physics and Chemistry, Nanoscience Center, University of Jyväskylä, Finland
- Wenping Hu - Key Laboratory of Organic Integrated Circuits, Ministry of Education & Tianjin Key Laboratory of Molecular Optoelectronic Sciences, Department of Chemistry, School of Science, Tianjin University, China
- Qiaofeng Yao - Key Laboratory of Organic Integrated Circuits, Ministry of Education & Tianjin Key Laboratory of Molecular Optoelectronic Sciences, Department of Chemistry, School of Science, Tianjin University, China

Background



Probing BSA Binding to Citrate-Coated Gold Nanoparticles and Surfaces

Scott H. Brewer, Wilhelm R. Glomm, Marcus C. Johnson, Magne K. Knag, and Stefan Franzen



Letter | Published: 09 August 2009

A quantitative fluorescence study of protein monolayer formation on colloidal nanoparticles

[Carlheinz Röcker](#), [Matthias Pötzl](#), [Feng Zhang](#), [Wolfgang J. Parak](#) & [G. Ulrich Nienhaus](#)

[Nature Nanotechnology](#) **4**, 577–580 (2009) | [Cite this article](#)

Review | [Open access](#) | Published: 19 July 2013


Interaction of nanoparticles with proteins: relation to bio-reactivity of the nanoparticle

[Shruti R Saptarshi](#), [Albert Duschl](#) & [Andreas L Lopata](#)

[Journal of Nanobiotechnology](#) **11**, Article number: 26 (2013) | [Cite this article](#)

77k Accesses | 792 Citations | 3 Altmetric | [Metrics](#)

Why this paper?



Lack of molecular-level understanding of nanomaterials-proteins interactions.

Hinders the development of precise nano-bio conjugates for advanced applications.

It probed the stoichiometric interactions of proteins and atomically precise nanoclusters at the specific binding sites, unlike the random adsorption of proteins on NPs.

Focused on the synergistic effects of both proteins and NCs.

Revealed detailed mechanistic insights like the electron transfer process, effects of structural modulation of protein as well as NCs.

Understanding of the specific binding interactions using MD simulations.

Introduction

- Atomically precise $\text{Au}_{25}(\text{p-MBS})_{18}$ (p-MBS = para-mercaptobenzenesulfonic acid)

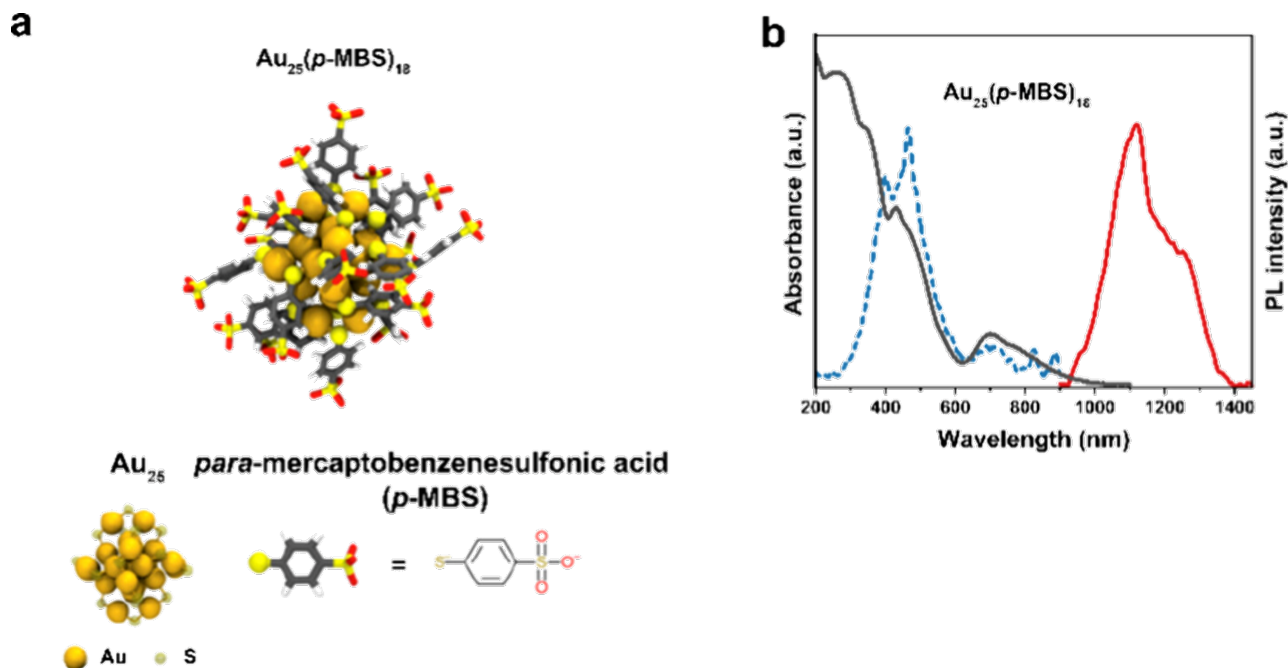


Figure 1. (a) Model structure of $\text{Au}_{25}(\text{p-MBS})_{18}$ (b) $\text{Au}_{25}(\text{p-MBS})_{18}$ (1100 nm emission under 470 nm excitation)

- Exhibits a NIR-II photoluminescence at 1100 nm under a broad excitation region (300-900) nm.
- 470 nm excitation includes both the intraband and interband transitions related with both Au atoms in Au_{13} core and S atoms in ligands, which correlate with LMCT process in the NIR-II emission of Au_{25} NCs
- Two lifetimes, 32.6 and 78.2 ns were simulated from the time-resolved spectroscopy of $\text{Au}_{25}(\text{p-MBS})_{18}$
- High negative surface charge at neutral pH conditions in water and distinct stabilities.

Introduction

- Bovine serum albumin (BSA) is used as the protein model
- Mature BSA consisted of 583 amino acids. It has three domains (I, II and III) and each domain has two sub domains A and B.

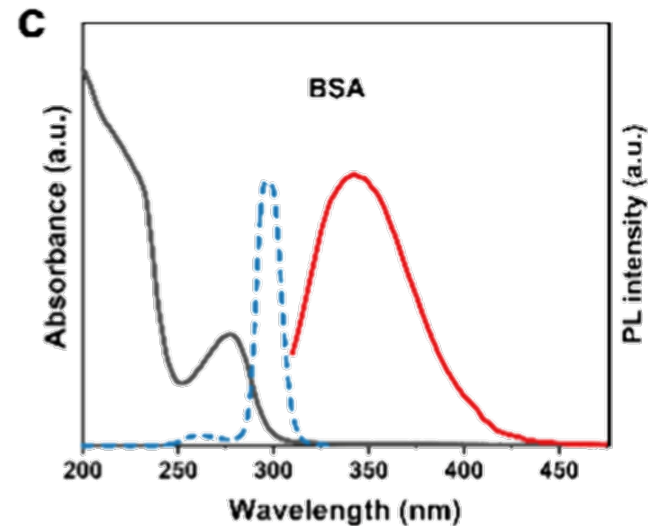
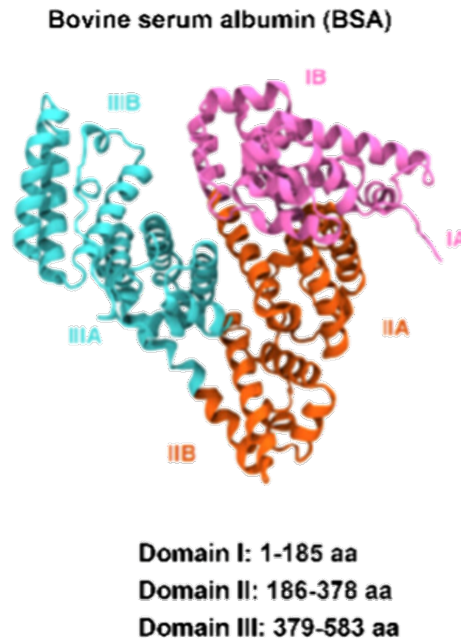


Figure 1. (a) Crystal structure of BSA with the domains (I, II, and III) and subdomains (A and B) depicted as ribbons in different colors. (c) BSA (350 nm emission under 290 nm excitation).

- The pristine fluorescence of BSA at 350 nm originates from tryptophan residues (Trp134 and Trp213) upon excited at 290 nm

Results and discussions

BSAprotein



$\text{Au}_{25}(\text{p-MBS})_{18}$

$\text{BSA}:\text{Au}_{25}(\text{p-MBS})_{18} = 0 \text{ to } 10$

PBS buffer, rt, 2 h

Protein-NC
conjugates

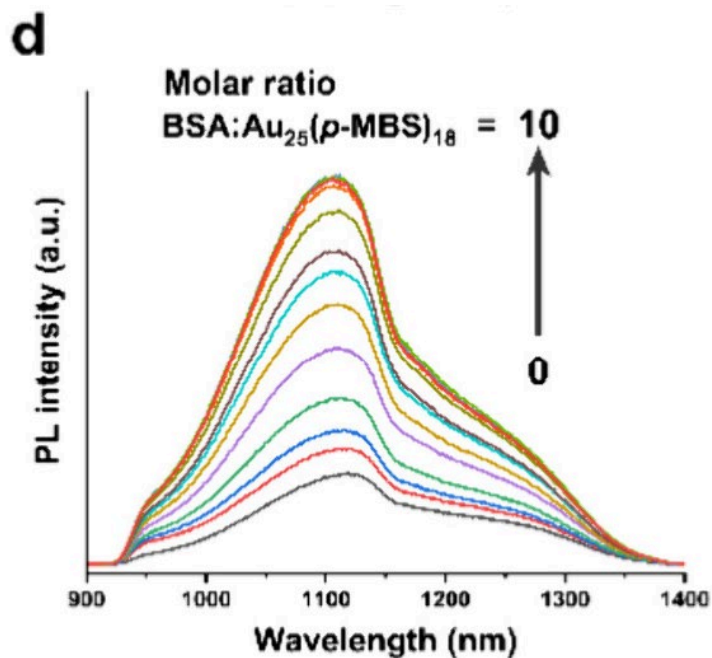


Figure 1. (d) Photoluminescence emission spectra of 0.01 mM $\text{Au}_{25}(\text{p-MBS})_{18}$ in the presence of different molar ratios of BSA (from 0 to 10 molar ratios of $\text{BSA}:\text{Au}_{25}(\text{p-MBS})_{18}$) with 470 nm excitation

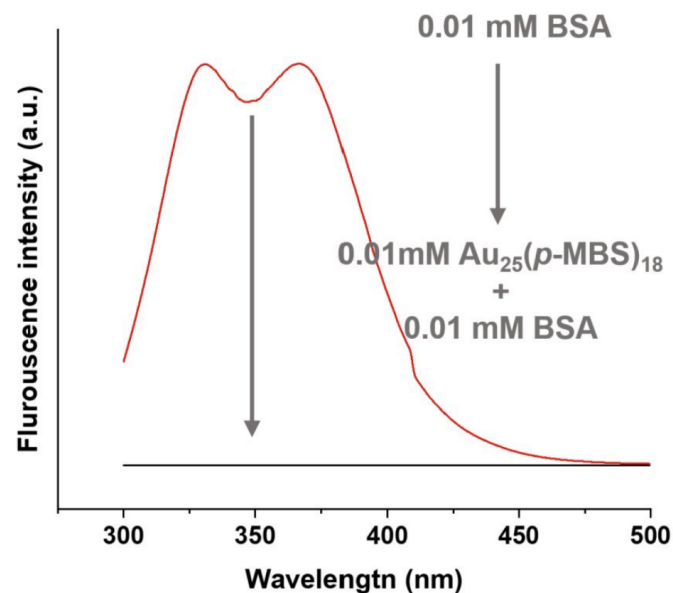


Figure S3. Photoluminescence emission spectra of 0.01 mM BSA and 0.01 mM BSA + 0.01 mM $\text{Au}_{25}(\text{p-MBS})_{18}$ under an excitation at 290 nm. $\text{Au}_{25}(\text{p-MBS})_{18}$ drastically quenched the fluorescence of BSA, supportive of the energy or electron transfer between BSA and $\text{Au}_{25}(\text{p-MBS})_{18}$.

Results and discussions

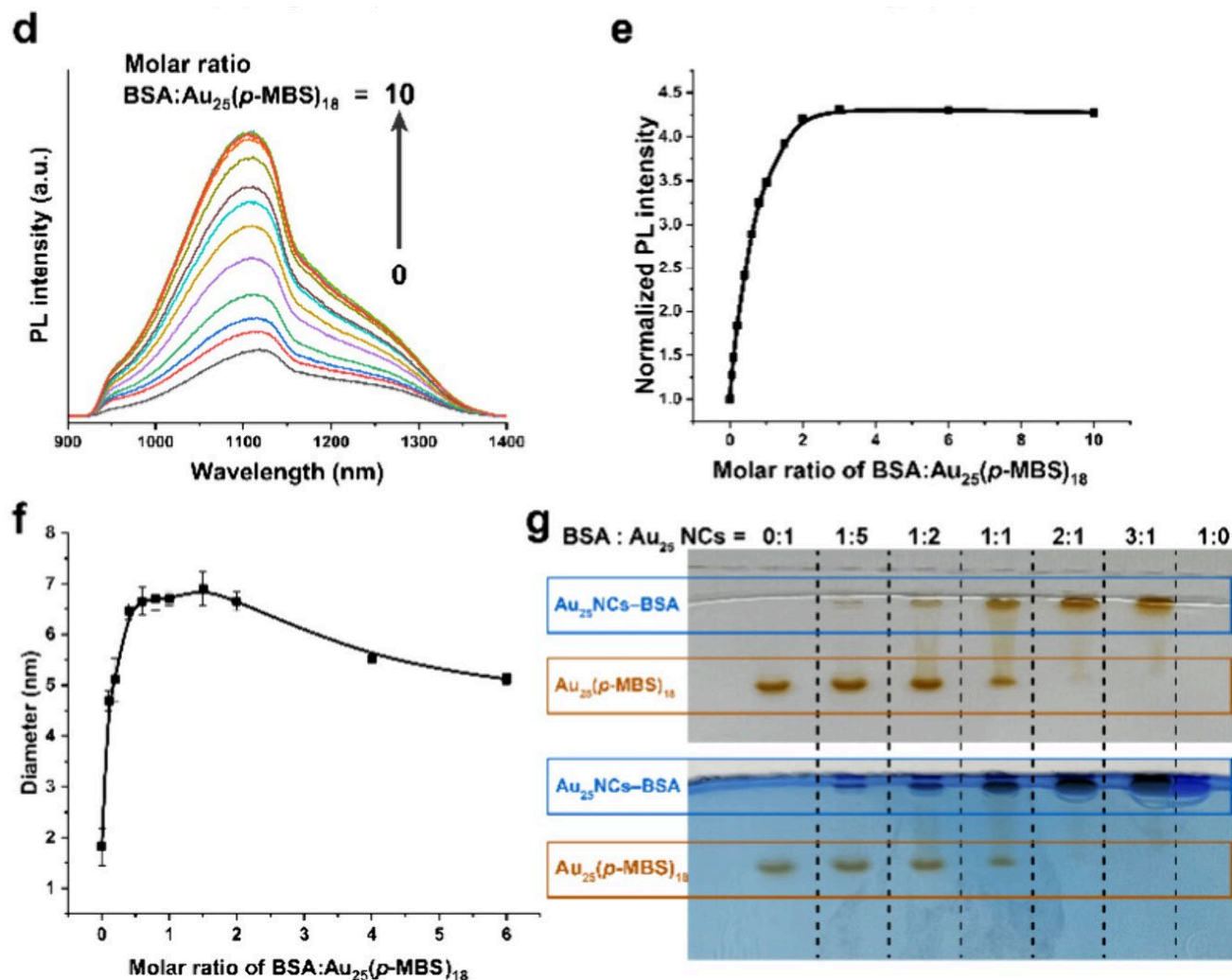


Figure 1. (d) Photoluminescence emission spectra of 0.01 mM $\text{Au}_{25}(\text{p-MBS})_{18}$ in the presence of different molar ratios of BSA (from 0 to 10 molar ratios of $\text{BSA}:\text{Au}_{25}(\text{p-MBS})_{18}$) with 470 nm excitation. (e) BSA: $\text{Au}_{25}(\text{p-MBS})_{18}$ molar ratio-dependent photoluminescence intensity of $\text{Au}_{25}(\text{p-MBS})_{18}$. (f) DLS graph of $\text{Au}_{25}(\text{p-MBS})_{18}$ at different $\text{BSA}:\text{Au}_{25}(\text{p-MBS})_{18}$ molar ratios. Error bars represent the standard deviation of triplicate independent measurements. (g) PAGE result of $\text{Au}_{25}(\text{p-MBS})_{18}$ + BSA at different $\text{BSA}:\text{Au}_{25}(\text{p-MBS})_{18}$ molar ratios. Coomassie blue was used to stain the gel for the visualization of BSA at the bottom panel. All of the experiments were conducted in 0.01 MPBS solution at pH 7.4 and room temperature.

Results and discussions

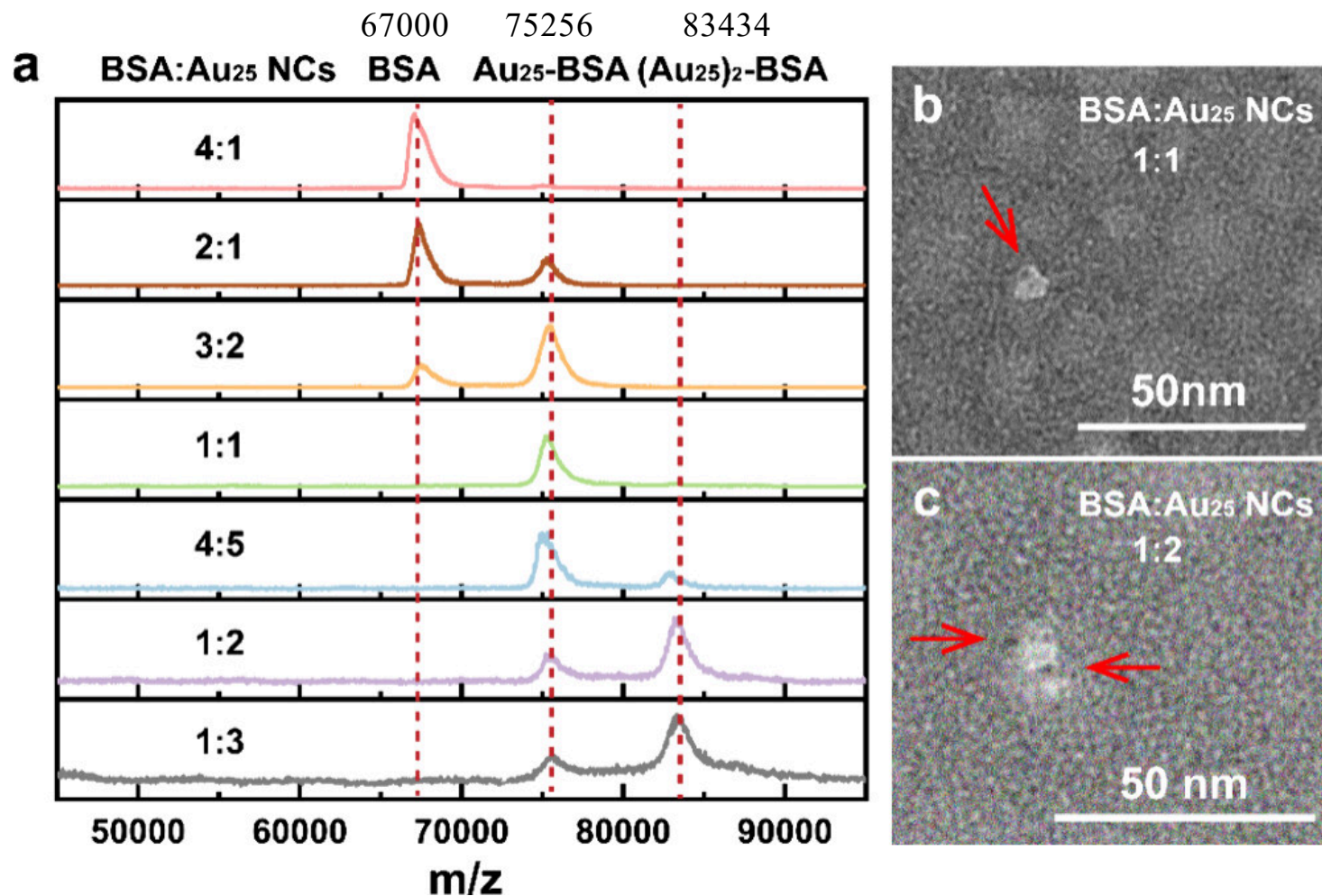


Figure 2. BSA possesses two binding sites for Au₂₅(p-MBS)₁₈ nanoclusters. (a) MALDI-TOF mass spectra of Au₂₅(p-MBS)₁₈ + BSA at different BSA: Au₂₅(p-MBS)₁₈ molar ratios. (b) Representative negative-stain TEM micrographs of Au NCs–BSA conjugates with 1:1 binding stoichiometry. (c) Representative negative-stain TEM micrograph of Au NCs–BSA conjugates with 2:1 binding stoichiometry.

Results and discussions

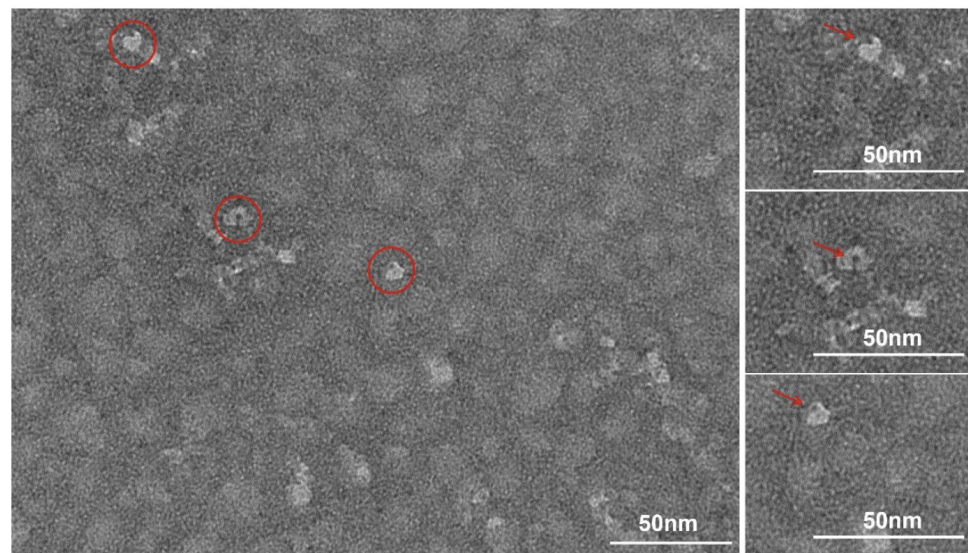
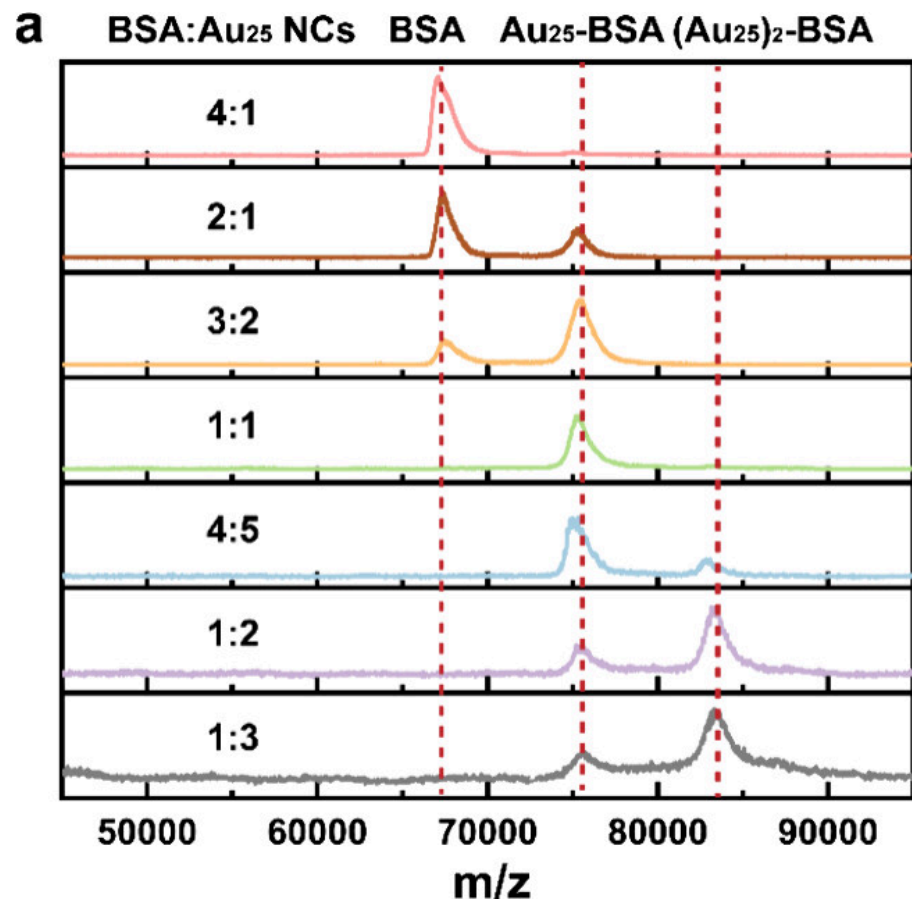


Figure S7. Negative-stain TEM micrographs of Au₂₅ NCs-BSA conjugates with 1:1 mixing ratio.

Figure 2. BSA possesses two binding sites for Au₂₅(p-MBS)₁₈ nanoclusters. (a) MALDI-TOF mass spectra of Au₂₅(p-MBS)₁₈ + BSA at different BSA:Au₂₅(p-MBS)₁₈ molar ratios.

Results and discussions

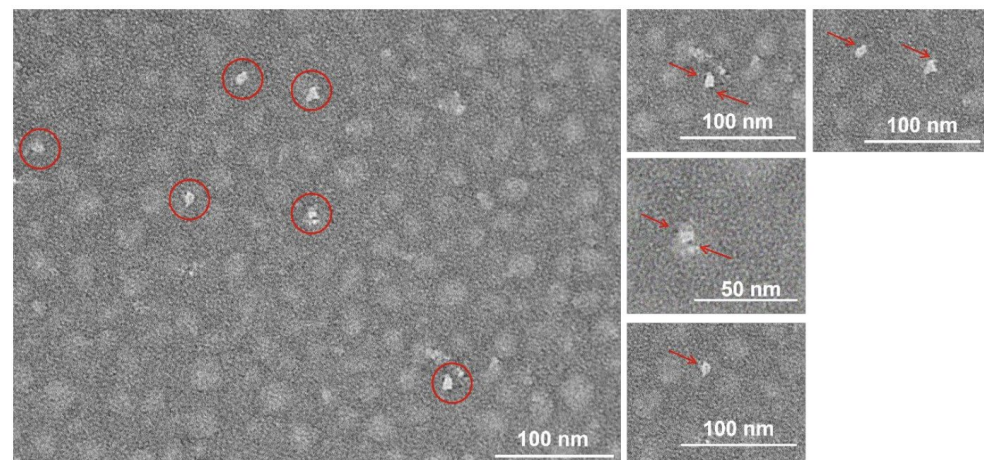
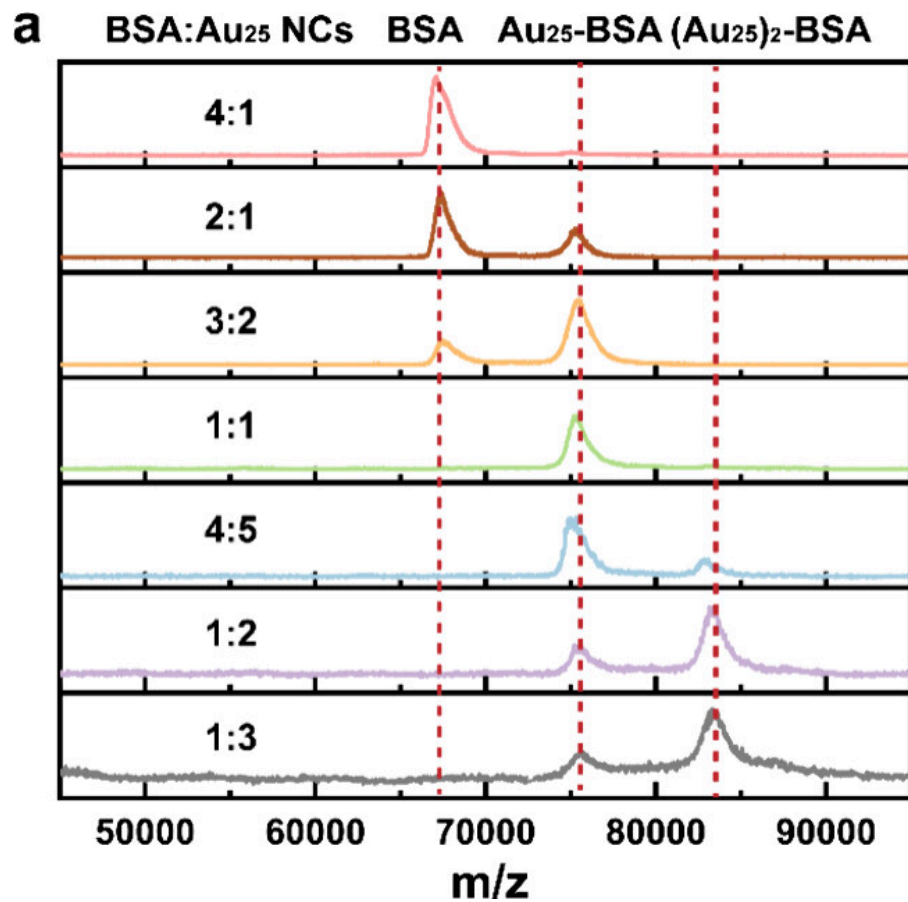


Figure S8. Negative-stain TEM micrographs of Au₂₅ NCs-BSA conjugates with 2:1 mixing ratio.

Figure 2. BSA possesses two binding sites for Au₂₅(p-MBS)₁₈ nanoclusters. (a) MALDI-TOF mass spectra of Au₂₅(p-MBS)₁₈ + BSA at different BSA: Au₂₅(p-MBS)₁₈ molar ratios.

Results and discussions

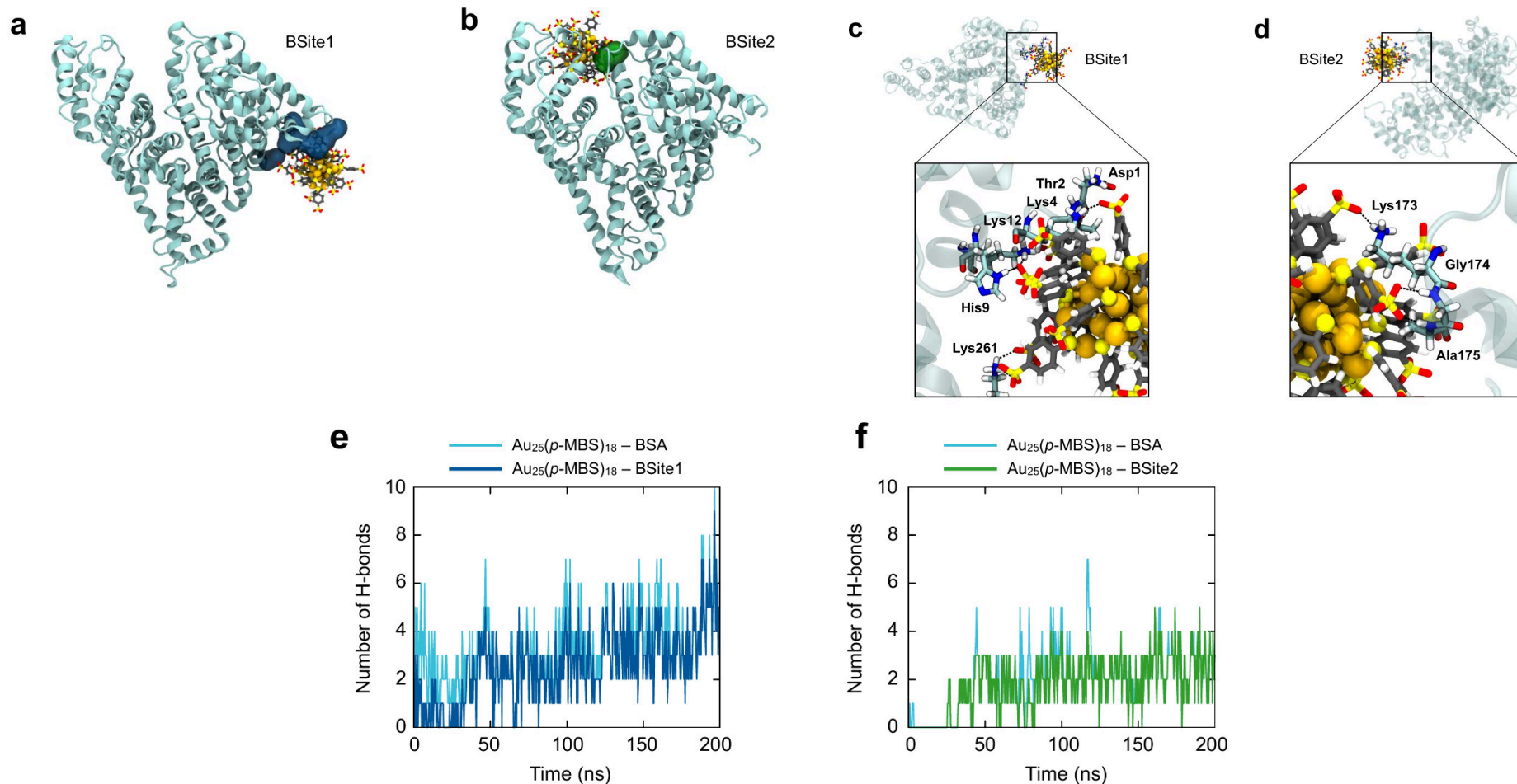


Figure 3. Computational modeling of the specific binding sites for $\text{Au}_{25}(\text{p-MBS})_{18}$ on BSA using 1:1 Au NC-BSA conjugates. (a and b) Representative snapshots from the 200 ns MD trajectory of $[\text{Au}_{25}(\text{p-MBS})_{18}]_1\text{-BSA}$ conjugate showing the identified binding sites on BSA in blue (BSite1) and green (BSite2) surfaces. (c and d) Representative zoom-in snapshots from the 200 ns MD trajectory showing the H-bonds (black dashed lines) formed between the ligand layer of $\text{Au}_{25}(\text{p-MBS})_{18}$ and residues from (c) BSite1 and (d) BSite2 on BSA. (e) Number of H-bonds formed between $\text{Au}_{25}(\text{p-MBS})_{18}$ and any region of BSA (cyan line) or specific residues that compose BSite1 (blue line) as a function of the simulation time. (f) Number of H-bonds formed between $\text{Au}_{25}(\text{p-MBS})_{18}$ and any region of BSA (cyan line) or specific residues that compose BSite2 (green line) as a function of the simulation time.

Results and discussions

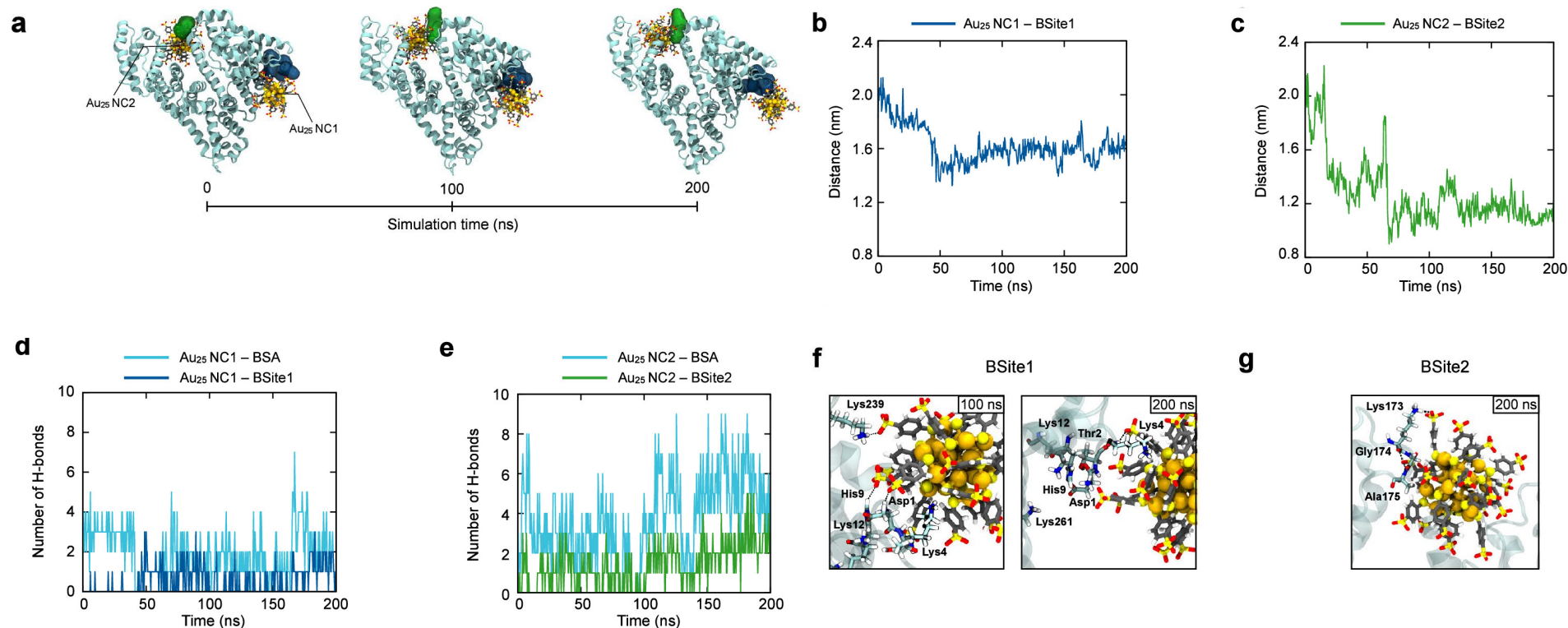


Figure 4. Computational modeling of the specific binding sites for $\text{Au}_{25}(\text{p-MBS})_{18}$ on BSA using 2:1 Au NCs-BSA conjugates. (a) Snapshots from the 200 ns MD trajectory of $[\text{Au}_{25}(\text{p-MBS})_{18}]_2$ -BSA showing the proximity of $\text{Au}_{25}(\text{p-MBS})_{18}$ nanoclusters (Au_{25} NC1 and Au_{25} NC2) with BSite1 (blue surface) and BSite2 (green surface) at different points of the simulation. (b) Distances between the center of mass (COM) of Au_{25} NC1 and COM of BSite1 during the simulation time. (c) Distances between COM of Au_{25} NC2 and COM of BSite2 during the simulation time. (d) Number of H-bonds formed between Au_{25} NC1 and any region of BSA (cyan line) or specific residues that compose BSite1 (blue line) as a function of simulation time. (e) Number of H-bonds formed between Au_{25} NC2 and any region of BSA (cyan line) or specific residues that compose BSite2 (green line) as a function of simulation time. (f and g) Zoom-in snapshots at different points of the 200 ns MD trajectory of $[\text{Au}_{25}(\text{p-MBS})_{18}]_2$ -BSA showing the H-bonds (black dashed lines) formed between the ligand layer of (f) Au_{25} NC1 and residues from BSite1, and (g) Au_{25} NC2 and residues from BSite2.

Results and discussions

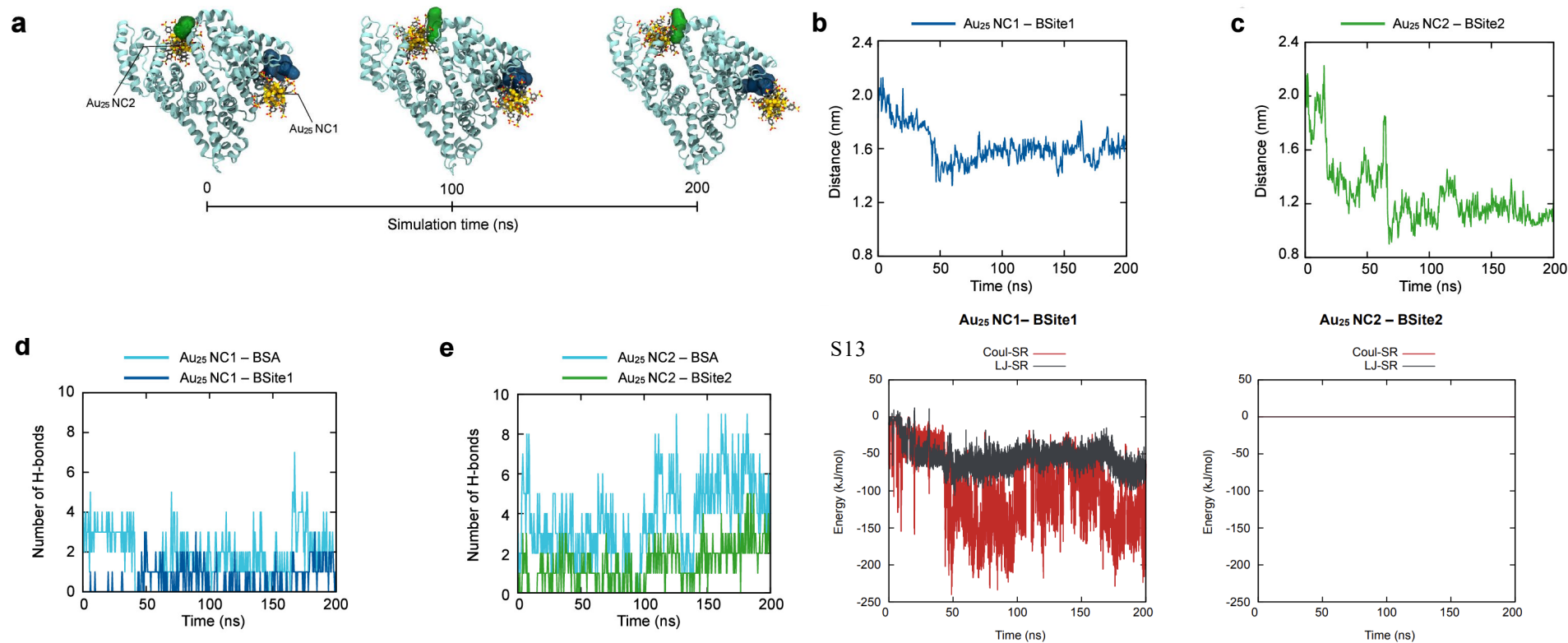


Figure 4. Computational modeling of the specific binding sites for Au₂₅(p-MBS)₁₈ on BSA using 2:1 Au NCs–BSA conjugates. (a) Snapshots from the 200 ns MD trajectory of [Au₂₅(p-MBS)₁₈]₂–BSA showing the proximity of Au₂₅(p-MBS)₁₈ nanoclusters (Au₂₅ NC1 and Au₂₅ NC2) with BSite1 (blue surface) and BSite2 (green surface) at different points of the simulation. (b) Distances between the center of mass (COM) of Au₂₅ NC1 and COM of BSite1 during the simulation time. (c) Distances between COM of Au₂₅ NC2 and COM of BSite2 during the simulation time. (d) Number of H-bonds formed between Au₂₅ NC1 and any region of BSA (cyan line) or specific residues that compose BSite1 (blue line) as a function of simulation time. (e) Number of H-bonds formed between Au₂₅ NC2 and any region of BSA (cyan line) or specific residues that compose BSite2 (green line) as a function of simulation time.

Figure S13. Interaction energies between two Au₂₅(p-MBS)₁₈ nanoclusters (Au₂₅ NC1 and Au₂₅ NC2) with different binding sites (BSite1 and BSite2) over 200-ns MD simulation for 2:1 Au₂₅(p-MBS)₁₈–BSA conjugates. Coul-SR and LJ-SR denote the average short-range Coulomb and Lennard-Jones energies, respectively.

Results and discussions

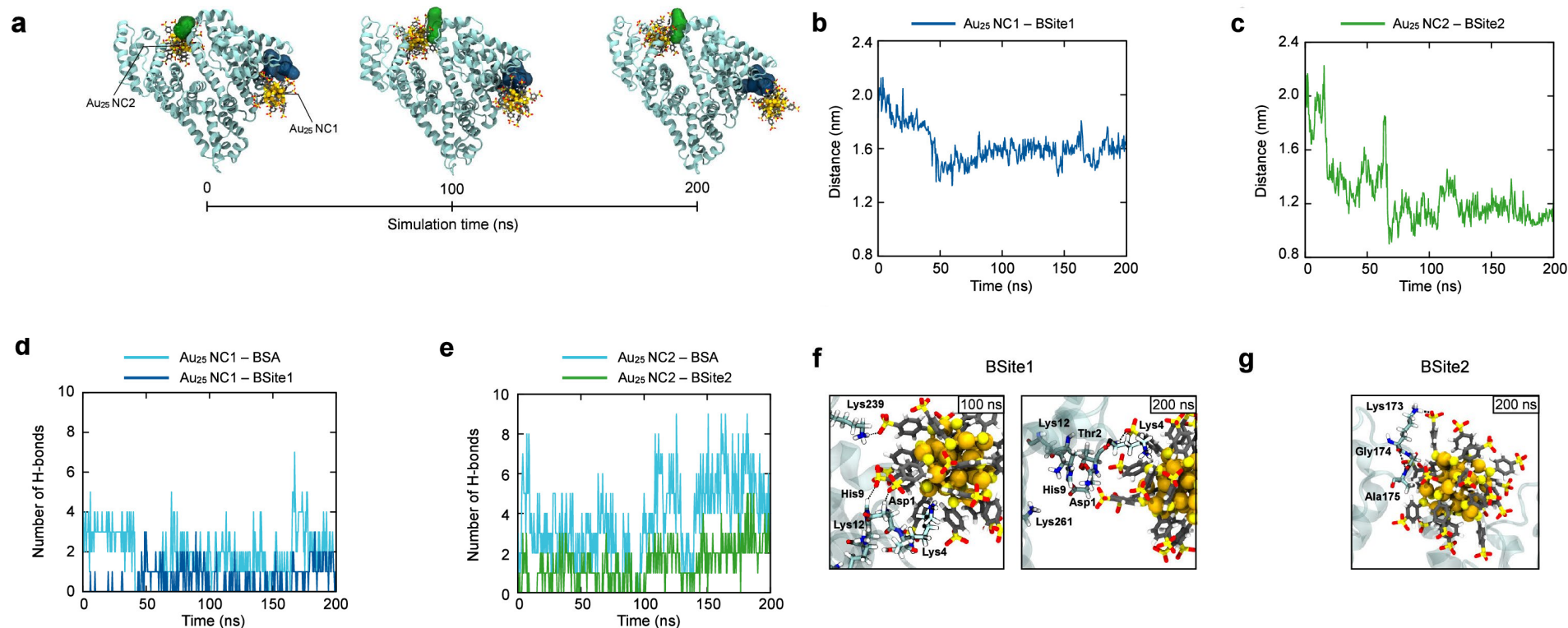


Figure 4. Computational modeling of the specific binding sites for $\text{Au}_{25}(\text{p-MBS})_{18}$ on BSA using 2:1 Au NCs-BSA conjugates. (a) Snapshots from the 200 ns MD trajectory of $[\text{Au}_{25}(\text{p-MBS})_{18}]_2$ -BSA showing the proximity of $\text{Au}_{25}(\text{p-MBS})_{18}$ nanoclusters (Au_{25} NC1 and Au_{25} NC2) with BSite1 (blue surface) and BSite2 (green surface) at different points of the simulation. (b) Distances between the center of mass (COM) of Au_{25} NC1 and COM of BSite1 during the simulation time. (c) Distances between COM of Au_{25} NC2 and COM of BSite2 during the simulation time. (d) Number of H-bonds formed between Au_{25} NC1 and any region of BSA (cyan line) or specific residues that compose BSite1 (blue line) as a function of simulation time. (e) Number of H-bonds formed between Au_{25} NC2 and any region of BSA (cyan line) or specific residues that compose BSite2 (green line) as a function of simulation time. (f and g) Zoom-in snapshots at different points of the 200 ns MD trajectory of $[\text{Au}_{25}(\text{p-MBS})_{18}]_2$ -BSA showing the H-bonds (black dashed lines) formed between the ligand layer of (f) Au_{25} NC1 and residues from BSite1, and (g) Au_{25} NC2 and residues from BSite2.

Results and discussions

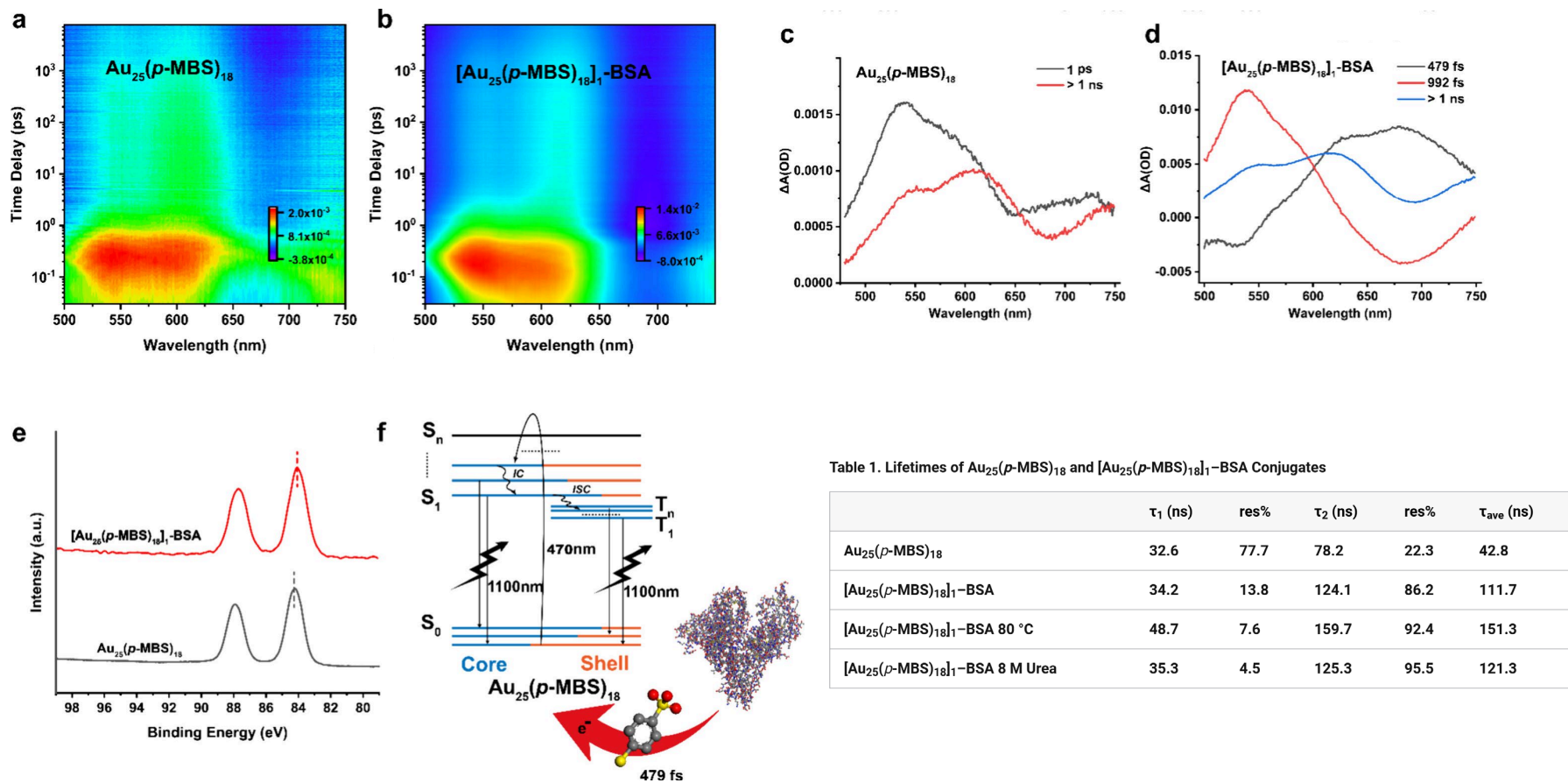


Table 1. Lifetimes of $\text{Au}_{25}(\text{p-MBS})_{18}$ and $[\text{Au}_{25}(\text{p-MBS})_{18}]_1\text{-BSA}$ Conjugates

	τ_1 (ns)	res%	τ_2 (ns)	res%	τ_{ave} (ns)
$\text{Au}_{25}(\text{p-MBS})_{18}$	32.6	77.7	78.2	22.3	42.8
$[\text{Au}_{25}(\text{p-MBS})_{18}]_1\text{-BSA}$	34.2	13.8	124.1	86.2	111.7
$[\text{Au}_{25}(\text{p-MBS})_{18}]_1\text{-BSA } 80^\circ\text{C}$	48.7	7.6	159.7	92.4	151.3
$[\text{Au}_{25}(\text{p-MBS})_{18}]_1\text{-BSA } 8\text{ M Urea}$	35.3	4.5	125.3	95.5	121.3

Figure 5. Electron transfer from BSA to Au NCs. (a and b) Ultrafast TA spectra of (a) $\text{Au}_{25}(\text{p-MBS})_{18}$ and (b) $[\text{Au}_{25}(\text{p-MBS})_{18}]_1\text{-BSA}$ conjugate. (c and d), Global fitting of the TA maps of (c) $\text{Au}_{25}(\text{p-MBS})_{18}$ and (d) $[\text{Au}_{25}(\text{p-MBS})_{18}]_1\text{-BSA}$ conjugate. (e) XPS spectra of $\text{Au}_{25}(\text{p-MBS})_{18}$ and $[\text{Au}_{25}(\text{p-MBS})_{18}]_1\text{-BSA}$ conjugate. (f) Schematic diagram of the excited state dynamics of $[\text{Au}_{25}(\text{p-MBS})_{18}]_1\text{-BSA}$ conjugate.

Results and discussions

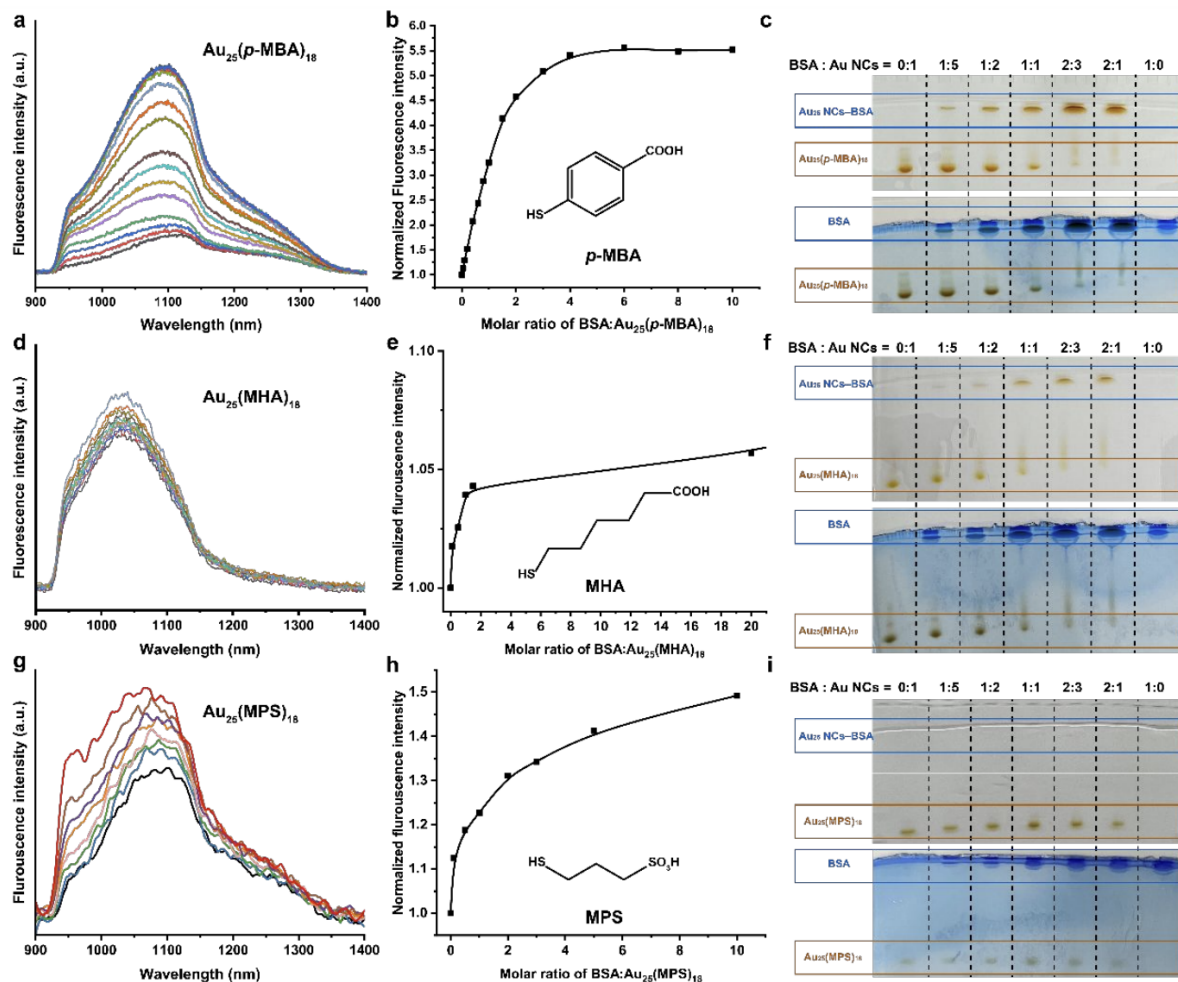


Figure S19. Ligand effect in the interactions between Au NCs and BSA. Photoluminescence emission spectra of 0.01 mM (a) $\text{Au}_{25}(\text{p-MBA})_{18}$, (d) $\text{Au}_{25}(\text{MHA})_{18}$, and (g) $\text{Au}_{25}(\text{MPS})_{18}$ in the presence of different concentrations of BSA with 470 nm excitation. BSA: Au_{25} NCs molar ratio dependent photoluminescence intensity of 0.01 mM (b) $\text{Au}_{25}(\text{p-MBA})_{18}$, (e) $\text{Au}_{25}(\text{MHA})_{18}$, and (h) $\text{Au}_{25}(\text{MPS})_{18}$. PAGE result of (c) $\text{Au}_{25}(\text{p-MBA})_{18}$, (f) $\text{Au}_{25}(\text{MHA})_{18}$, and (i) $\text{Au}_{25}(\text{MPS})_{18}$ + BSA at different BSA: Au_{25} NCs molar ratios. All the experiments were conducted in 0.01 MPBS solution at pH 7.4 and room temperature.

Results and discussions

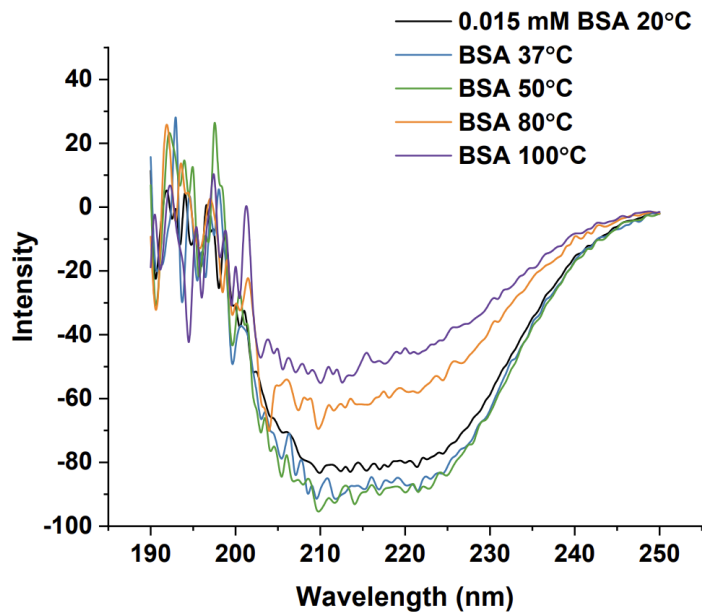


Figure S21. Temperature-dependent CD spectra of BSA.

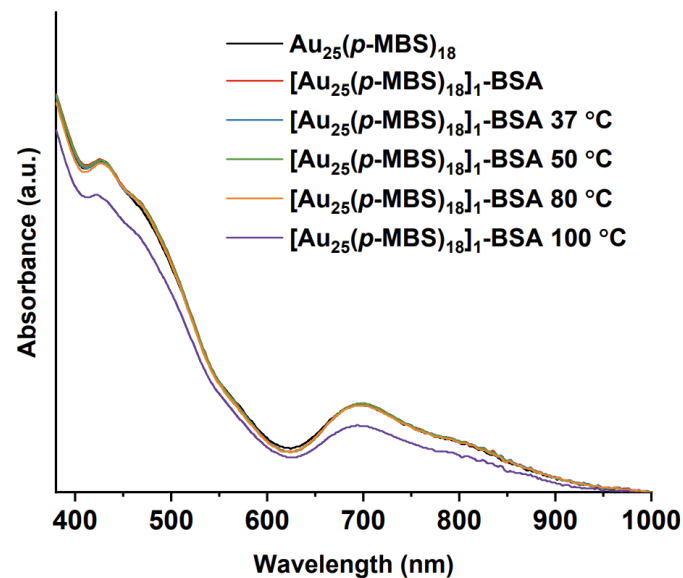


Figure S23. Temperature-dependent UV-vis spectra of $\text{Au}_{25}(\text{p-MBS})_{18}$ -BSA conjugates.

Results and discussions

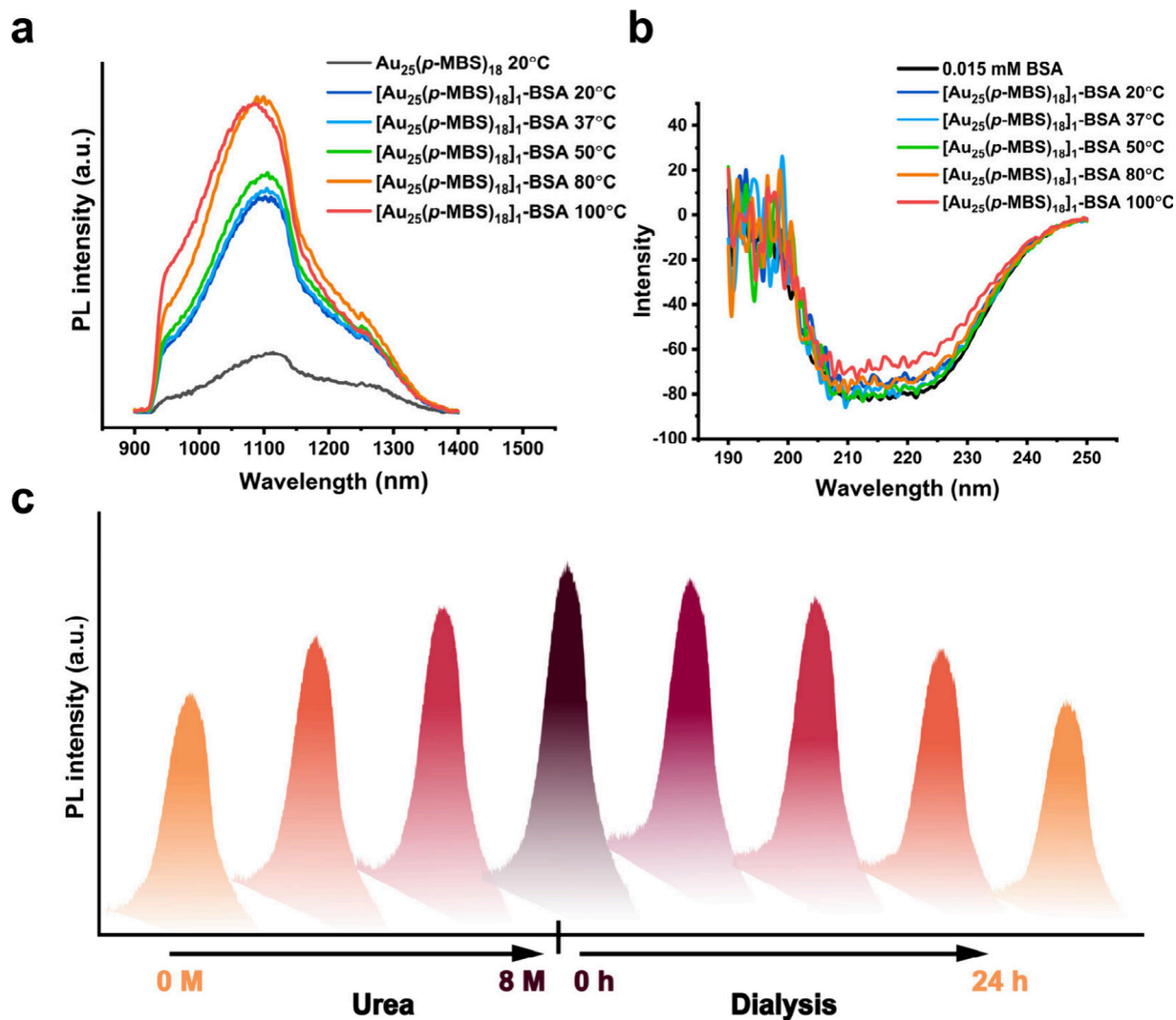


Figure 6. Synergistic effect of the Au NCs-BSA conjugate. (a) Temperature-dependent photoluminescence spectra of the $[\text{Au}_{25}(\text{p-MBS})_{18}]_1\text{-BSA}$ conjugate. (b) Temperature-dependent CD spectra of the $[\text{Au}_{25}(\text{p-MBS})_{18}]_1\text{-BSA}$ conjugate. (c) Urea concentration-dependent photoluminescence spectra of the $[\text{Au}_{25}(\text{p-MBS})_{18}]_1\text{-BSA}$ conjugate. All the experiments were conducted in 0.01 MPBS solution at pH 7.4 and room temperature unless otherwise indicated.

Conclusions

- This study revealed the stoichiometric and specific and selective binding interactions of atomically precise nanoclusters with proteins.
- Molecularly precise $[\text{Au}_{25}(\text{p-MBS})_{18}]_x\text{-BSA}$ conjugates ($x = 1$ or 2) are formed without structural disruption of any individual component.
- Specific binding sites and binding affinity are understood by MD simulations.
- TA spectroscopic studies revealed that electron transfer from BSA to NC enhances the NIR-II luminescence of the NCs.
- The $[\text{Au}_{25}(\text{p-MBS})_{18}]_1\text{-BSA}$ conjugate exhibits a synergistic effect, in which $\text{Au}_{25}(\text{p-MBS})_{18}$ enhances the stability of BSA, and structural changes in BSA can manipulate the electronic structure of the NCs.